2019 EAGE ANNUAL
81ST CONFERENCE + EXHIBITION
LONDON | THE UNITED KINGDOM

Tu_P01_08

Robust FWI Updates in the Presence of Cycle Skipping

J. Ramos-Martinez[1]*, A. Valenciano[1], X. Jiang[1], N. Chemingui[1]

[1] Petroleum Geo-Services

Summary

Full Waveform Inversion (FWI) success depends on producing seamless short- and long-wavelength model updates while avoiding cycle skipping. In its traditional implementation, FWI risks converging to an inaccurate result if the data lacks sufficient low frequencies or the starting model is far from the true one. Additionally, the model updates may display a reflectivity imprint before the long-wavelength features are fully recovered. A solution to these fundamental challenges combines the quadratic form of the Wasserstein distance (W2-norm) for measuring the data misfit with a robust implementation of a velocity gradient. The W2-norm reduces the risk of cycle skipping whereas the velocity gradient effectively eliminates the reflectivity imprint and emphasizes the long-wavelength model updates. We illustrate the performance of the new solution on a field survey acquired offshore Brazil. There, we demonstrate how FWI successfully updates the earth model and resolves a high-velocity carbonate layer that was missing from the starting model.

Introduction

Classic FWI (Tarantola, 1984) can produce velocity updates with the reflectivity imprint (high-wavenumbers) before the long-wavelength components (low-wavenumbers) of the model are constructed (Mora, 1989). To mitigate the problem, practitioners follow cumbersome data selection strategies. The operational challenge and the fact that only reflections from deep targets might be available have motivated the development of more sophisticated FWI gradients. Their objective is to produce low-wavenumber updates form transmitted and reflected events (e.g., Xu et al., 2012; Zhou et al., 2015; Ramos-Martínez et al., 2016).

Moreover, the misfit function based on the L2-norm measures the difference between the recorded and modeled oscillatory signals on a point-by-point basis. It constrains FWI to use starting models that allow the wave simulation within half of the period of the recorded data. In cases where the starting model does not satisfy this requirement, the inversion may suffer from cycle skipping and converge to a wrong velocity model. Again, this limitation can be overcome by applying laborious data selection strategies. The events with the lowest frequencies and the nearest offsets are used first. In subsequent stages, broader frequency bandwidths and increased offset ranges are considered. However, in many cases, the acquired seismic data do not have enough low frequencies to comply with the half-period condition. Moreover, in complex geological settings where salt, carbonates, or basalt are present a small error in the location of the reflectors would lead to large kinematic errors. Hence, there is an incentive to use different metrics than the L2-norm for quantifying the data misfit (e.g., Engquist et al., 2016; Métivier et al., 2016; Qiu et al., 2017).

Here, we combine the quadratic form of the Wasserstein distance (W2-norm) to measure the data misfit with a robust implementation of the velocity gradient. Our method introduces a weighted velocity sensitivity kernel derived from the impedance and velocity parameterization of the objective function (Ramos–Martinez et al., 2016). It effectively separates the migration isochrones produced by the specular reflectivity from the components created by transmitted arrivals. Our numerical implementation (Qiu et al., 2017) uses an encoding scheme based on a logistic function that assures the positiveness and mass conservation conditions required by the optimal transport theory.

Theory

FWI is a nonlinear inverse problem that matches modeled data to the recorded field data (Tarantola, 1984). Generally, a least-squares objective function is used for measuring the data misfit. Here we estimate the data difference using the W2-norm:

$$J = \sum_s \sum_r W_2^2(\tilde{u}, \tilde{d}) \qquad (1)$$

where $\tilde{u}(t)$ and $\tilde{d}(t)$ are encoded versions of the modeled and field data. The W2-norm and the resulting Frechet derivative are explained in Qiu et al. (2017). In addition, we use the logistic function to encode both the field and modeled data.

To produce long-wavelength updates, we adapted the equations for the velocity gradient (Ramos-Martínez et al., 2016) to work with the W2 misfit function. The dynamic weight implementation of the velocity kernel was translated to the equivalent expressions such that the first-order time derivatives of the source and residual wavefields are computed before the adjoint source backward propagation. The resulting velocity kernel has the form:

$$G_v(x) = \frac{1}{A(x)} \int \left[W_1(x,t) \frac{1}{V(x)^2} S(x,t) R(x, T-t) + W_2(x,t) \nabla S(x,t) \nabla \hat{R}(x, T-t) \right] dt$$

where $S(x,t)$ is the source wavefield, and $R(x,t)$ is the wavefield computed from the adjoint-state equation using the time reversal of a preconditioned adjoint source. $\hat{R}(x, T-t)$ results from applying

the inverse of the preconditioning operator to the adjoint wavefield, and $A(x)$ is the illumination term. The weights $W_i(x,t)$ were designed to suppress the unwanted specular reflectivity (migration isochrones) as the solution of an optimization problem. Ramos–Martinez et al. (2018) provided more details on the velocity gradient derivation.

Figure 1 shows the sensitivity kernels for different combinations of the L2-norm, W2-norm and the FWI gradients. They were computed for a source-receiver pair in a layer where velocity increases with depth. Notice that the W2 velocity kernel accentuates the long-wavelength components compared to the L2 velocity kernel.

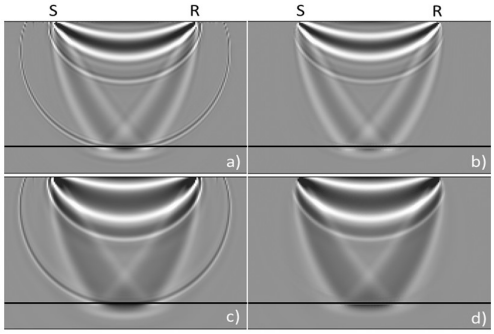

Figure 1 *Sensitivity kernels of a source-receiver pair in a model with a V(z) layer over a half-space for a) L2-norm and cross-correlation FWI gradient, b) L2-norm and FWI velocity gradient, c) W2-norm and cross-correlation gradient, and d) W2-norm and velocity gradient.*

Field data from offshore Brazil

We applied the new FWI algorithm to a field data survey acquired in the Ceará basin, offshore Fortaleza, Brazil. The acquisition comprised 14 deep tow multisensor streamers with a maximum inline offset of 8 km. The signal-to-noise ratio was good at frequencies as low as 2.5 Hz; the maximum frequency used in the inversion was 8 Hz. The inversion data window contained a mix of transmitted and reflected events. The legacy velocity model (Figures 2a, 3a, and 4a) missed a package of near-seafloor carbonates that created deeper distortions of the seismic image (Figure 6a) as well as cycle skipping (Figure 5a). Due to the shallow water (around 50 m) and the data's contamination by multiples, the use of reflection tomography for updating the near surface layers was limited. Meanwhile, the high contrast carbonates (about 3300 m/s from a nearby well log Figure 3) limited the penetration of the refracted energy to approximately 1.2 km depth.

Figures 2b and 2c show the inverted models obtained in a first stage using the L2- and W2-norms. In both cases, we used the velocity gradient to minimize the high-wavenumber artefacts produced by the multiples. The L2-norm inversion gave an update in the wrong direction due to cycle skipping. In contrast, the W2-norm yielded an increase in velocity where the carbonates are expected.

We validated the FWI results by comparing synthetic and recorded shot gathers (Figure 5). Figure 5a shows a recorded shot gather overlaying by the synthetic using the starting model clearly showing the cycle skipping at intermediate and long-offsets. Figure 5b shows the comparison using the L2-norm inverted model. The match of near offsets improves, but the intermediate and far offsets suffer from cycle skipping. In contrast, the W2-norm synthetics (Figure 5c) show better match at all offset ranges.

After resolving the cycle skipping problem, we continued the inversion using L2-norm FWI (Figures 2d, 3b, and 4b). The high-velocity carbonates are now resolved, and the match between the field and the modeled traces is suitable for all offsets (Figure 5d). The velocity increase was corroborated with well log data. Figure 3a and 3b show the starting and final FWI models for a line in the proximity of the well. The final FWI model matches the well trend capturing the spatial variability of the carbonates. Finally, reflection tomography was applied to update the deeper part of the model. Figures 5a and 5b show the Kirchhoff migrated images overlaying the starting and final velocity models. Note the improvement in the continuity of the deeper reflectors from the starting to the final models.

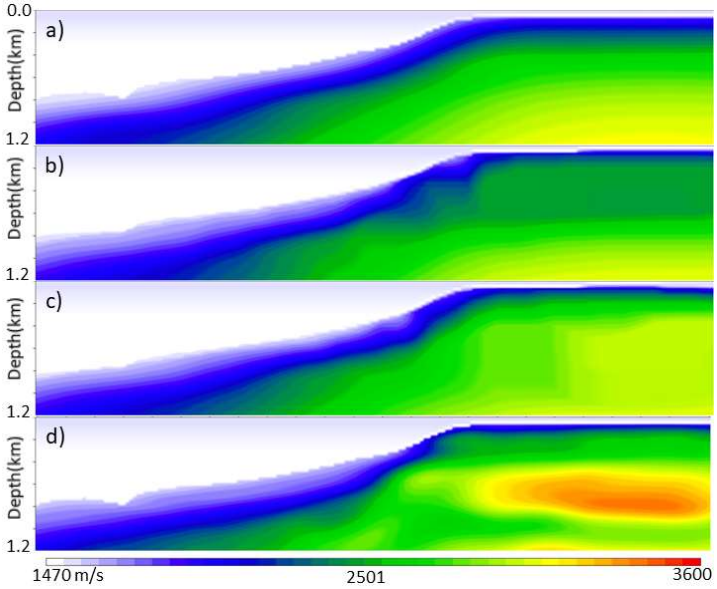

Figure 2 *Model comparisons in the crossline direction a) starting model, b) FWI model using L2-norm, c) FWI model using the W2-norm, and (d) FWI model produced by cascading the W2-norm and L2-norm.*

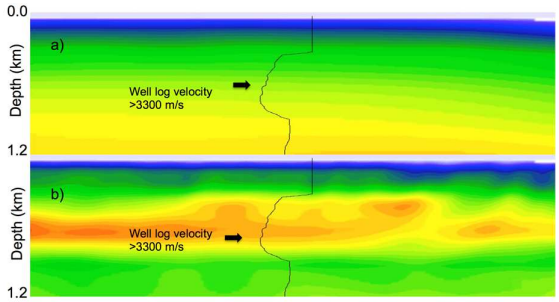

Figure 3 *Model comparisons in the inline direction at the proximity of the well: a) starting model and b) Final FWI model produced by cascading the W2-norm and L2-norm.*

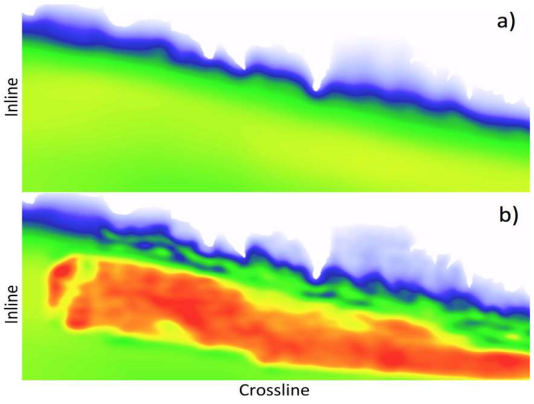

Figure 4 *Model comparisons at the depth of 800 m: a) starting model and b) Final FWI model produced by cascading the W2-norm and L2-norm.*

Conclusions

We combined a robust implementation of the velocity gradient and the optimal transport norm (W2) to solve the FWI cycle skipping problem and retrieve the long-wavelength velocity updates. The proposed solution expands the use of FWI for velocity model building as it reduces the dependency on accurate starting velocity models and therefore relaxes the requirements on ultra-low-frequency data. We illustrated the advantages of the new algorithm on a field data survey where it resolved high-velocity carbonates that were missing from the starting model. Well log data corroborated the carbonates presence and validated the FWI result. The final velocity model improved the image of both shallow and deep structures.

Acknowledgements

We thank PGS MultiClient for permission to use the field data. We also thank Mikhail Orlovich for the assistance with the field data processing, and Lingyun Qiu, Yunan Yang, Dan Whitmore, and Faqi Liu for helpful discussions.

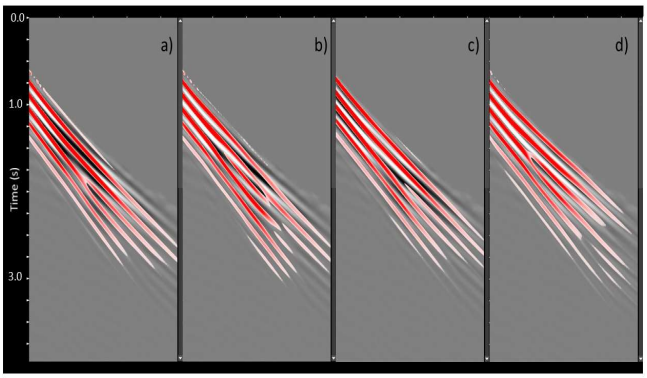

Figure 5 *Comparison of field records and synthetic shot gathers computed with: a) starting model, b) FWI model using L2-norm, c) FWI model using W2-norm, and d) W2-norm followed by L2-norm. The positive amplitudes of the synthetic traces (red) should match the corresponding positive amplitudes of the recorded traces (black) if the model is accurate.*

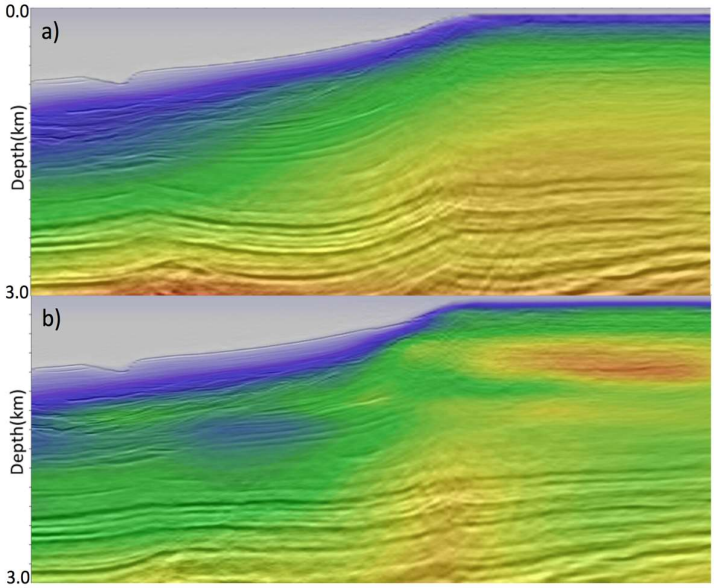

Figure 6 *Kirchhoff migrated image overlaying the velocity model: a) starting model, b) final FWI model after deeper tomography. Note the improvement in the continuity of the deeper reflectors from starting to the final model.*

References

Engquist, B., Froese, B.D. and Yang, Y. [2016] Optimal transport for seismic full waveform inversion: Communications in Mathematical Sciences, **14**, 2309-2330.

Métivier, L., Brossier, R., Mérigot Q., Oudet, E. and Vireux, J. [2016] Measuring the misfit between seismograms using an optimal transport distance: application to full waveform inversion, Geophysical Journal International, **205**, 345-377.

Mora, P., [1989] Inversion = migration + tomography: Geophysics, **54** (12), 1575-1586.

Qiu, L., Ramos-Martinez, J., Valenciano, A.A., Yang Y. and Enquist, B. [2017] Full-waveform inversion with an exponentially encoded optimal-transport norm, 87th SEG Annual International Meeting, Expanded Abstracts, 1286-1290.

Ramos-Martinez, J., Crawley, S., Zou, Z., Valenciano, A.A., Qiu, L. and Chemingui, N. [2016] A robust gradient for long wavelength FWI updates, 76th EAGE Conference & Exhibition, Extended Abstracts, Th SRS2 03.

Ramos-Martínez, J., Qiu L., Kirkebø J., Valenciano A.A. and Yang Y. [2018] Long-wavelength FWI updates beyond cycle skipping. SEG Technical Program Expanded Abstracts 2018: pp. 1168-1172.

Tarantola, A., [1984] Inversion of seismic reflection data in the acoustic approximation, Geophysics, **49**, 1259-1266.

Xu, S., Wang, D., Chen, F., Zhang, Y. and Lambaré, G. [2012] Full waveform inversion for reflected seismic data, 74th EAGE Conference & Exhibition, Extended Abstracts, W024.

Zhou, W., Brossier, R., Operto S. and Vireux, J. [2015] Full waveform inversion of diving waves for velocity model building with impedance inversion based on scale separation, Geophysical Journal International, **202**, 1535-1554.